SAR Computation inside Fetus by RF Coil during MR Imaging Employing Realistic Numerical Pregnant Woman Model

Satoru KIKUCHI[†a)], *Student Member*, Kazuyuki SAITO[††], Masaharu TAKAHASHI[††], *Members*, Koichi ITO[†], *Fellow*, and Hiroo IKEHIRA[†††], *Nonmember*

SUMMARY   This paper presents the computational electromagnetic dosimetry inside an anatomically based pregnant woman models exposed to electromagnetic wave during magnetic resonance imaging. The two types of pregnant woman models corresponding to early gestation and 26 weeks gestation were used for this study. The specific absorption rate (SAR) in and around a fetus were calculated by radiated electromagnetic wave from highpass and lowpass birdcage coil. Numerical calculation results showed that high SAR region is observed at the body in the vicinity of gaps of the coil, and is related to concentrated electric field in the gaps of human body such as armpit and thigh. Moreover, it has confirmed that the SAR in the fetus is less than International Electrotechnical Commission limit of 10 W/kg, when whole-body average SARs are 2 W/kg and 4 W/kg, which are the normal operating mode and first level controlled operating mode, respectively.
key words: *magnetic resonance imaging (MRI), birdcage coil, pregnant woman, fetus, specific absorption rate (SAR)*

1.   Introduction

In recent years, various types of imaging systems have been employed for diagnosis of diseases on the medical field. They are ultrasonic pulse-echo technique and X-ray computed tomography, positron emission tomography, magnetic resonance imaging (MRI) etc. In those techniques, MRI is one of diagnostic modalities to obtain detail images of the human tissues and anatomical structures, without using ionizing radiation. The MRI system is composed of several important units including radio frequency (RF) technologies such as RF coil [1]. Several kinds of RF coils are developed and selected according to the imaging portion of the body. During the magnetic resonance (MR) imaging, the RF coil radiates pulsing electromagnetic (EM) waves (RF pulses) to the human body and in response receives the nuclear magnetic resonance signals emitted from the nuclei, which constitutes the human body. Here, according to shape of the RF pulses, various types of images inside the body can be obtained. In general, although widths of the RF pulses are narrow, their amplitudes are not so low. Therefore, it is necessary to estimate the specific absorption rate (SAR) in the

human body due to the radiated EM energy from the RF coils.

Until now, the SAR evaluation in the human head has been studied during MR imaging [2]–[6], and the restriction of SAR for the safety of patients has been established as the International Electrotechnical Commission (IEC) standard [7]. Recently, MR imaging is employed not only for the head but also for various portions of the body, because the MRI system tends to generation of high quality images and reduction of imaging time. Especially, in this paper, the SAR distributions in a pregnant woman and her fetus are investigated. In general, an ultrasound diagnostic system is used for the medical examination of the pregnant woman. However, the MR imaging is sometimes chosen for the medical reasons, when the diagnosis with ultrasound is unclear for diagnosis of fetal anomaly [8]–[10]. Moreover, several researchers have been suggested that there is uncertain regarding the risk posed by MR imaging to the fetus [11].

Therefore, over the past few years, several studies have been made on the SAR evaluation of pregnant woman and her fetus due to the radiated EM energy from the RF coil [12]–[14]. In these studies, the SAR estimation was investigated about the local average SAR and the average SAR of fetus by employing abdomen model. Hence, the evaluation on the local peak SAR in fetus and pregnant woman was hardly investigated. Furthermore, in some studies, fetus model used for the calculation was a simple structure model that had not anatomical structure. Meanwhile, a realistic whole-body pregnant woman model including an anatomically fetus model for EM dosimetry has been developed by the National Institute of Information and Communications Technology (NICT), Japan and Chiba University [15]. The authors studied the fundamental investigations on the SAR calculation using the whole-body pregnant woman model by RF coil [16]. Additionally, our previous study regarding the SAR evaluation in pregnant woman exposed to the EM wave from communication devices are described in [17]. Consequently, the SAR inside a fetus is calculated using a whole-body voxel model of a pregnant woman positioned close to a dipole antenna and planar inverted F antenna.

In this paper, the SAR distributions in the pregnant woman and her fetus exposed to the EM waves from the RF coil were calculated employing the two types of different pregnancy stage high-resolution whole-body pregnant woman models. As the purpose of this paper is concerned, it is necessary to discuss both viewpoints of the local SARs

and the average SARs in detail. In addition, two types of birdcage coil were employed for these calculations. In Sect. 2, the two types of woman models of different pregnancy stage and two types of configurations of a birdcage coil for MRI system are explained. In Sect. 3, the SAR distributions in these models are discussed. Finally, conclusions are presented in Sect. 4.

2. Numerical Calculation Method and Calculation Models

2.1 Calculation Method

In the numerical calculation, the electric field in and around the coil is analyzed by the finite difference time domain (FDTD) method [18] and the EM energy absorption rate (SAR) is calculated from the following equation:

$$SAR = \frac{\sigma}{\rho} E^2 \qquad [W/kg] \qquad (1)$$

where σ is the conductivity of the tissue [S/m], ρ is the density of the tissue [kg/m^3], and E is the electric field (rms) [V/m]. The SAR takes a value proportional to the square of the electric field generated inside the human body and is equivalent to the heating source generated by the electric field in the human tissue. In addition, it has been confirmed that the result of numerical calculation corresponded with measurement result employing tissue-equivalent solid phantom [19].

2.2 Realistic Woman Models

As stated above in this paper, the SAR distributions on two types of realistic woman models are calculated. Here, the realistic high-resolution whole-body voxel model of an adult Japanese female average figure, developed at NICT [20] is used for the calculation of the pregnant woman in early period (Model A). The size of fetus (embryo) in early period is very small, hence it is difficult to confirm pregnancy status. Therefore, it is considered that the person, who does not notice her own pregnancy state, uses MRI. Moreover, the 26th gestational week pregnant woman model (Model B) [15]–[17] is employed as one example of late pregnancy stages. In order to develop this model, first, the fetus model is developed from the MR images of a pregnant woman in the 26th gestational week. The fetus model consists of six organs including fetal body, fetal brain, fetal eyes, amniotic fluid, placenta, and uterus wall. Next, the abdomen of the Model A is expanded following the standard shape and structure of the pregnant woman. Finally, these two models are combined and adjusted following the comments from medical doctors. In addition, the more detailed explanations regarding the development of pregnant woman model are described in [15].

Figures 1(a) and (b) show Model A and B, respectively. These high resolution models are composed of 2 mm × 2 mm × 2 mm cubical voxel. The physical properties of

External view   Coronal plane   Sagittal plane
(a) Pregnant woman model in early period composed of 51 organs (Model A).

External view   Coronal plane   Sagittal plane
(b) Pregnant woman model in the 26th gestational week composed of 56 organs including fetal tissues (Model B).
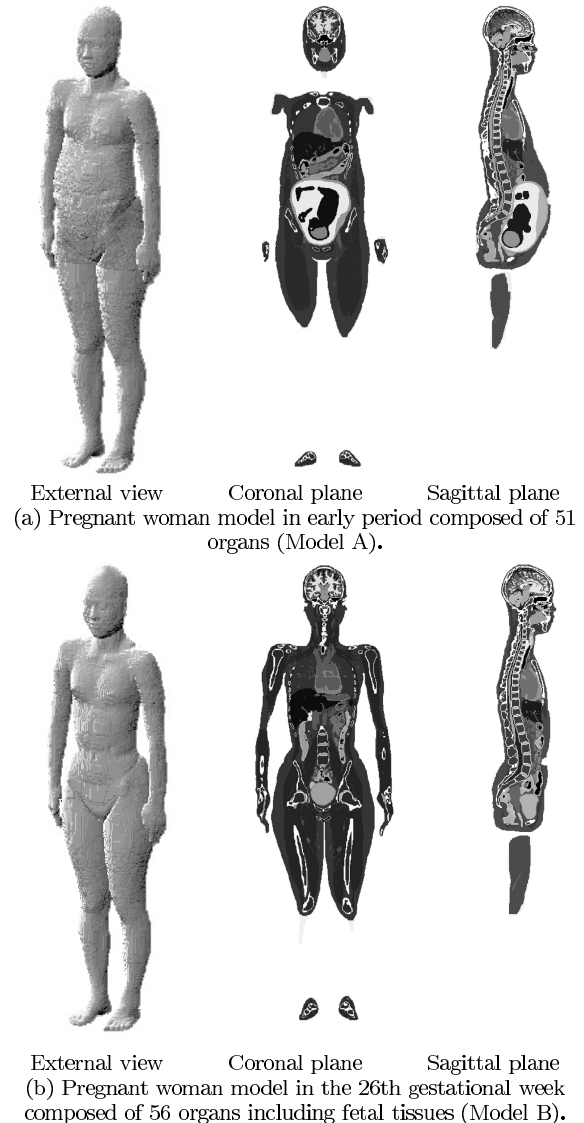
Fig. 1 Realistic woman models from [16].

these models are determined from [13], [21]–[23], except dielectric properties of fetal brain and fetal body. Here, it has been found that dielectric properties at microwave frequency band depended on tissue water contents [24]. Consequently, the dielectric properties of fetal brain and fetal body adjusted to account for the higher water content in comparison with similar adult tissues. These properties were decided with correction method by the difference of water content in the tissue. The procedure for determining values were previously discussed by Hand et al. [13]. Table 1 summaries a part of the parameters around the abdomen of pregnancy and her fetus.

2.3 Calculation Models of RF Coil

In this paper, a birdcage coil is employed as one of the most fundamental RF coils for MRI system. The birdcage coil is often used as both the transmission of RF pulse and re-

Table 1 Example of physical properties of pregnant woman and her fetus at 64 MHz.

	Density ρ[kg/m^3]	Relative permitivity ε_r	Conductivity [S/m]
Maternal body			
Muscle	1,040	72.0	0.71
Fat	928	13.6	0.07
Skin	1,100	84.4	0.46
Blood	1,060	86.5	1.21
Bone cortical	1,990	16.7	0.06
Bone cancellous	1,040	18.2	0.11
Lung	655	56.2	0.41
Liver	1,050	80.6	0.45
Stomach	1,050	85.8	0.88
Colon	1,044	94.7	0.64
Small intestine	1,044	118.3	1.59
Ovary	1,048	106.8	0.69
Uterus wall	1,052	92.1	0.91
Amniotic fluid	1,000	97.3	2.07
Placenta	1,060	86.5	1.21
Fetal body			
Body	1,040	94.2	0.92
Eyes	1,009	69.1	1.50
Brain	1,030	97.2	0.76

Fig. 2 Two types of birdcage coil with RF shield.

Fig. 3 FDTD calculation model.

ception of NMR signal, and is categorized into two types by the difference of the position of loaded capacitors; one is a highpass birdcage coil, and the other is a lowpass birdcage coil [1]. Figures 2(a) and (b) show the highpass birdcage coil with RF shield and lowpass birdcage coil with RF shield, respectively. The operating frequency of the coil is around 64 MHz in both cases, which is used in the generic 1.5 T MRI systems to excite the nuclei in the human body for imaging. These coils consist of two end rings and eight legs, whose widths are 10 mm, and are composed of perfect electric conductors for calculations. The diameter and the length of the coil are 600, 700 mm, respectively, so that the realistic woman model can be inserted. In order to reduce radiation of RF energy to outside of the coil, the coils are surrounded by RF shield which is also modeled as perfect electric conductor. A cylindrical RF shield, with an internal diameter of 740 mm and a length of 1,260 mm, has been located lateral to the coil. The dimensions of the coil and the RF shield were determined based on [13], [14], [25].

Here, the capacitors were loaded into the end rings on the highpass birdcage coil in Fig. 2(a), and into the legs on the lowpass birdcage coil in Fig. 2(b). In order to determine the capacitances, "birdcage builder [26]," which calculates the resonance frequency of the birdcage coil by the equivalent electrical circuit model, was employed. Values for capacitors to resonate both coils at 64 MHz were 15.27 pF for the highpass birdcage coil and 4.47 pF for the lowpass birdcage coil. In addition, two feeding points were employed in these calculations and the phase difference between two ports is 90 degree. This excitation method is called "Quadrature excitation" and can generate clear MR image by using circular polarized field [1].
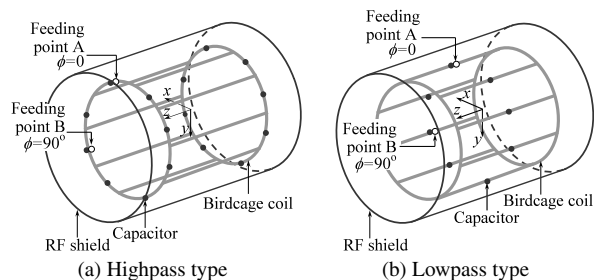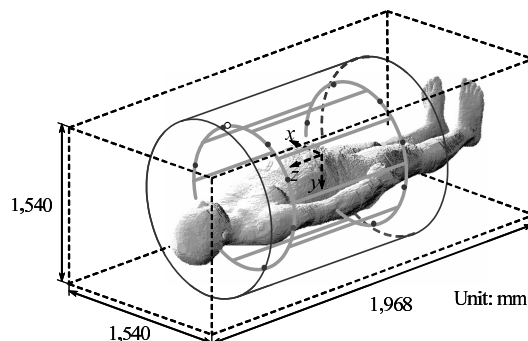
2.4 Numerical Calculation Model

Figure 3 indicates FDTD calculation model including the realistic woman model. As an example of the model, the Model B is inserted into highpass birdcage coil. There are several possibilities for the coil position, because it is considered that the position of the coil is not the same for each imaging. Previously, the relationship of several position of the RF coil to the SAR was calculated [27]. However, in this paper, the coil was placed the center of uterus in Model A, and placed center of fetal brain in Model B. In order to calculate the whole-body of the woman models, a large analytical region was required and a super technical server (Hitachi SR11000) in the Institute of Media and Information Technology, Chiba University was employed. In the numerical calculations, the uniform grid size inside of the shield including the woman model is 2.0 mm. The non-uniform mesh is used for the outside of the shield, because most of the EM waves are not emitted outward by the shield.

The parameters used in the FDTD calculations are listed in Table 2. In addition, steady state analysis is performed by enforcing a continuous sinusoidal wave of electric field on the feeding gaps to calculate the SAR distribution in the model. Moreover, the coordinate origin is the center of calculation model. In the previous study, we investigated on the SAR evaluation inside the tissue-equivalent solid phantom using surface coil, the effectiveness of calculation technique is confirmed by comparison with an experiment result [28].

Table 2 Parameters for FDTD calculations.

Cell size [mm]	$\Delta x, \Delta y$	2.0, 2.0
(Minimum)	Δz	2.0 (const.)
Cell size [mm]	$\Delta x, \Delta y$	5.6, 5.6
(Maximum)	Δz	2.0 (const.)
Analytical space $x \times y \times z$ [cell]		$534 \times 534 \times 984$
Time step [ps]		3.8
Absorbing boundary condition		PML (8 layers)

3. SAR Distribution in the Abdomen of Pregnant Woman Models

In the actual MRI system, the various pulse sequences are employed according to the imaging region and type. However, in this paper, the SARs in the pregnant woman and her fetus were calculated by exciting the continuous sinusoidal wave at feeding point, because the radiation power of each pulse sequence was not clear. Here, in order to simplify conversion of radiation power, the SAR values are normalized by 1.0 W radiation power from the coil in all cases. In addition, the radiation power was calculated by a surface integral of poynting vector on closed surface surrounding the coil.

3.1 Comparison of the SAR Distributions in Model A with the Two Types of RF Coils

Figures 4(a)–(h) show the calculated SAR distributions inside the Model A by employing the highpass and lowpass birdcage coil, respectively. The observation planes are the sagittal plane (yz-plane) including the uterus, and the coronal plane (xz-plane) around the center of the uterus. Moreover, positions of observation line A-A', B-B', C-C', and D-D' are indicated in the Figs. 4(a)–(d). In this paper, Model A (the non-pregnant woman model) is assumed as the early period of pregnancy. Therefore, the SAR inside the uterus and ovary were observed in place of fetal tissue, because the fetus or embryo was very small in the early period [29].

As shown in Figs. 4(b) and (d), the SAR distributions on the coronal plane are observed unsymmetrical tendency in comparison with the left side ($-225\,\text{mm} < z < 0$) and right side ($0 < z < 225\,\text{mm}$). Moreover, it was confirmed that a tendency of the SAR distribution changes when we observe the coronal plane of other positions. Because it was considered that the tendency is influenced by two points of feeding, a symmetry of SAR distributions was confirmed in the case of one point of feeding model. Moreover, from Figs. 4(a)–(d), relatively high SAR values are observed around the skin, muscle, etc which have a high electrical conductivity and located close to the surface of the maternal body. The tendency can be confirmed in Figs. 4(e)–(h), except fat tissue which is low electrical conductivity. Moreover, a high SAR values are observed inside the thigh ($x = 0$, $-100 < z < -300\,\text{mm}$ in Figs. 4(b) and (d)) and armpit ($x = \pm200\,\text{mm}$, $z = 400\,\text{mm}$ in Figs. 4(b) and (d)). This is due to the concentrated electric field at those narrow gaps. In comparison with the SAR distributions due to the EM energy from the highpass and lowpass birdcage coil, we observed comparatively high SAR values in the vicinity of each positions of feeding point and loaded capacitor. Here, according to the result that confirmed all SAR distributions, it was found that this phenomenon is dependent on whether an electric field concentrates on existing gap of the human body and a coil.

Meanwhile, the SAR in the uterus and the ovary (around $15 < y < 60\,\text{mm}$, $-50 < z < 50\,\text{mm}$ in Figs. 4(a) and (c), around $-40 < x < 25\,\text{mm}$, $-50 < z < 50\,\text{mm}$ in Figs. 4(b) and (d)) are low compared to the maternal surface of skin and muscle tissue. In addition, low SAR value is observed at the uterus (around $15 < y < 60\,\text{mm}$ in Figs. 4(e) and (f), around $-40 < x < 25\,\text{mm}$ in Figs. 4(g) and (h)) due to the attenuation of EM energy in the muscle tissue ($-150 < x < -80\,\text{mm}$, $80 < x < 140\,\text{mm}$ in Figs. 4(f) and (h)). Moreover, compared with the SAR in the uterus and the ovary by different coil type, it is observed that there is hardly a difference. From these result, it has been confirmed that the SARs in the uterus and the ovary are low, because these areas are placed in deep region of the body.

3.2 Comparison of the SAR Distributions in Model B with the Two Types of RF Coils

Figures 5(a)–(h) show the calculated SAR distributions inside the Model B by use of the highpass and lowpass birdcage coil, respectively. The observation planes are the sagittal plane (yz-plane) including the center of the fetal head, and are the coronal plane (xz-plane) around the center of fetal body. Moreover, positions of observation line A-A', B-B', C-C', and D-D' are indicated in the Figs. 5(a)–(d).

As shown in Fig. 5, relatively high SAR values are observed around the maternal surface and unsymmetrical tendency are observed by the effect of two points feeding. Moreover, it is observed that the SAR at the amniotic fluid is also relatively high. Especially, relatively high SAR values are observed at the upper and lower portions of amniotic fluid (around $y = -100$, $z = -50$, $150\,\text{mm}$ in Figs. 5(a) and (c), around $x = 0$, $z = -50\,\text{mm}$ and $x = 100\,\text{mm}$, $50 < z < 200\,\text{mm}$ in Figs. 5(b) and (d)). In addition, as the Figs. 5(e)–(h) indicate, it has found that the SAR in the amniotic fluid near the fetal tissue is relatively high. This is because the electrical conductivity of amniotic fluid is almost 1.5–2.0 times higher than other tissues, as listed in Table 1. In addition, the SAR distributions around the boundary of each tissue were precipitously varied due to the heterogeneous structure.

However, the SAR in the fetus (around $-20 < y < 50\,\text{mm}$ at Figs. 5(e) and (g), around $-50 < x < 15\,\text{mm}$ in Figs. 5(f) and (h)) is the low, which is compared to the values of maternal body. Moreover, maximum SAR value within fetus is less than 1.0% of that of the maternal body. From these results, it has been confirmed that the SAR in the fetus is attributed to the attenuation of EM energy in the amniotic fluid which is high conductivity. Here, we focused attention on the power deposition of amniotic fluid, and the power deposition of the amniotic fluid for the total values was cal-
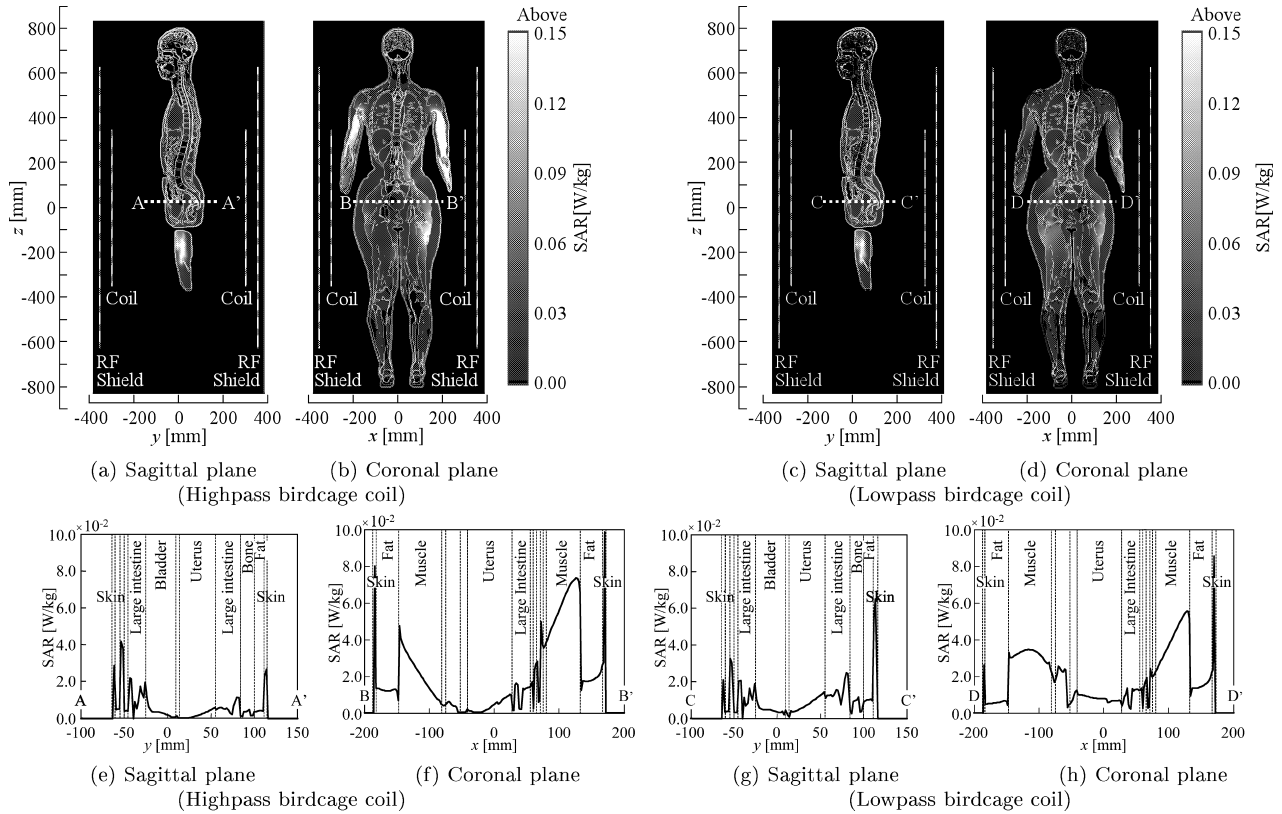
Fig. 4 Calculated SAR distributions inside Model A due to radiated EM waves from two types of birdcage coil. Figuers (a), (b), (e), and (f) are the SARs employing highpass birdcage coil. Figures (c), (d), (g), and (h) are the SARs employing lowpass birdcage coil.

culated. As a result, these values were 7% in highpass birdcage coil and 5% in lowpass birdcage coil. Therefore, in the case of the temperature rise analysis, we considered that it is necessary to examine the effect of the amniotic fluid.

3.3 Whole-Body and Fetal Average SAR

Figure 6 illustrates the calculated results of whole-body average SAR and fetus or uterus average SAR inside the Models A and B. The comparisons of the average SAR by the differences among types of coils and models are shown below.

1) Comparison with the average SAR of two types of coils
In both Model A (assumed early period pregnancy) and Model B (26th gestational week pregnant woman), whole-body average SARs employing a highpass and lowpass birdcage coil are almost the same value. This is because the coil dimension which is an EM wave source to irradiate for the human body is same. However, the uterus average SAR in Model A of lowpass birdcage coil is higher than that of highpass birdcage coil. This is because the positions of uterus and ovary in the calculation model approached feeding gaps and gaps of loaded capacitor. In Model B, fetus average SARs have no so much of a difference between highpass and lowpass birdcage coil. This is due to the attenuation of

EM energy in the amniotic fluid existing around the fetus.

2) Comparison with the average SAR of two types of pregnant woman models
As shown in Fig. 6, the uterus and the fetus average SARs are lower than whole-body average SARs in each case. This is because the fetus and uterus are located at deep region in the maternal body. Moreover, whole-body average SAR in Model A is higher than that in Model B. Here, the weight of these models are 52.4 kg (in Model A) and 58.8 kg (in Model B), respectively. From these results, it has been suggested that whole-body average SAR depend on weight of human body, when irradiation source of the EM wave was the same size as the coil.

3.4 Local Average SAR in the Fetus

Figure 7 represents calculated peak 10 g average SARs of the uterus and ovary inside Model A, and of the fetus including fetal body, fetal brain, and fetal eye balls inside Model B. Here, the 10 g average SAR presents the average value of SAR in 10 g of tissue and is widely employed for EM dosimetry in this field. The calculation method for 10 g average SAR employed 10 g cubical averaging volume in accordance with IEEE standard C95.3-2002 [30] Annex E. The uterus and ovary inside the Model A, fetal tissues in-

(a) Sagittal plane   (b) Coronal plane
(Highpass birdcage coil)

(c) Sagittal plane   (d) Coronal plane
(Lowpass birdcage coil)

(e) Sagittal plane   (f) Coronal plane
(Highpass birdcage coil)

(g) Sagittal plane   (h) Coronal plane
(Lowpass birdcage coil)
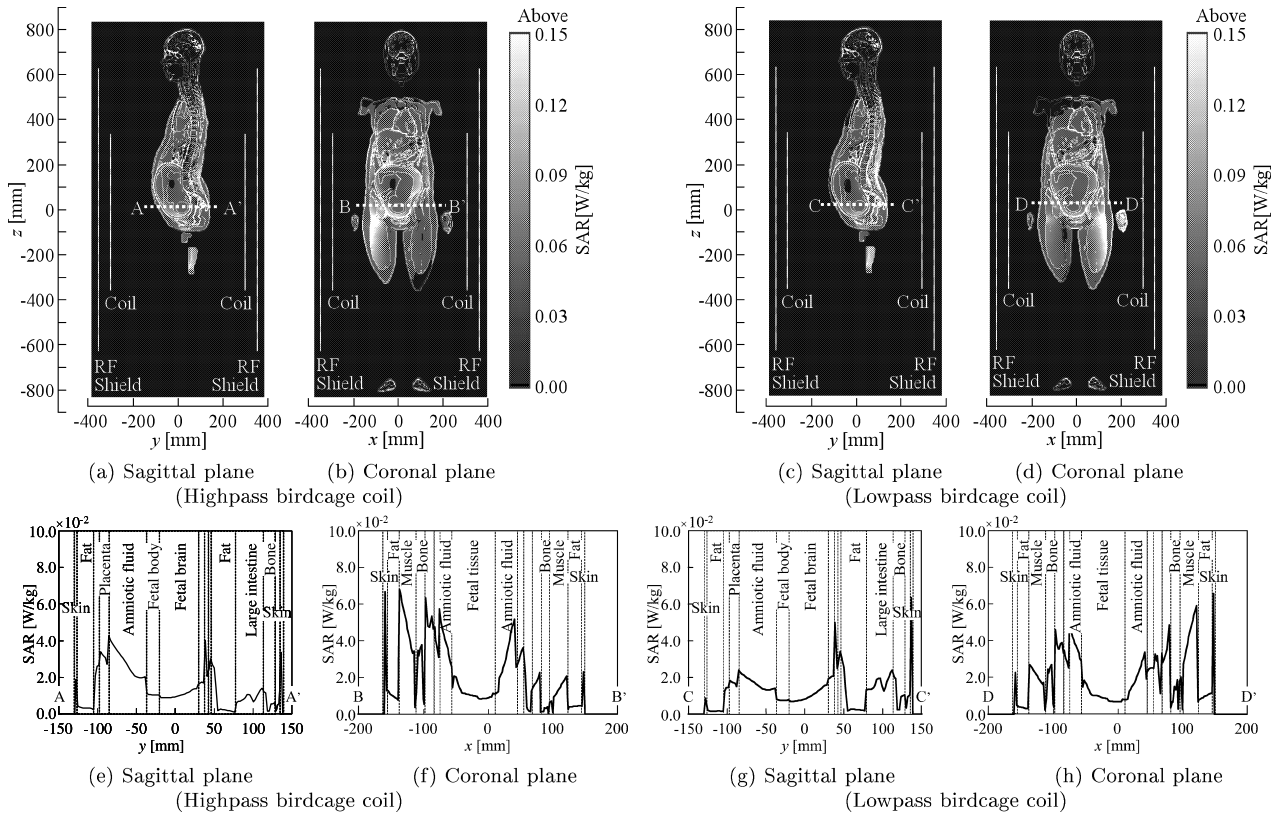
Fig. 5 Calculated SAR distributions inside Model B due to radiated EM waves from two types of birdcage coil. Figures (a), (b), (e), and (f) are the SARs employing highpass birdcage coil. Figures (c), (d), (g), and (h) are the SARs employing lowpass birdcage coil.
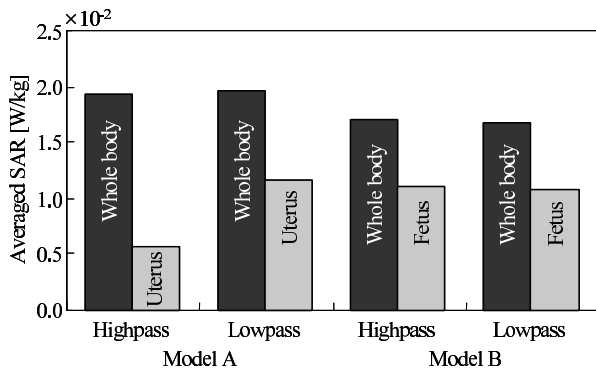
Fig. 6 Averaged SARs inside two types of pregnant woman models due to the EM energy from highpass and lowpass birdcage coil.
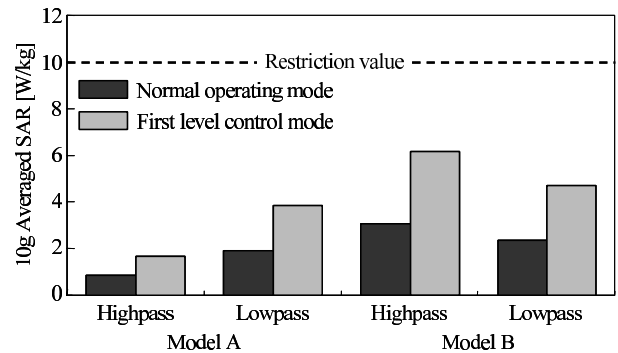
Fig. 7 10g averaged-SARs inside the fetus or uterus of the models exposed to EM wave from highpass and lowpass birdcage coil.

side the Model B are included with more than 80% for the calculation of peak average SAR. In addition, in order to compare with restriction value of the IEC 60601-2-33 [7], the SAR values are normalized to the whole-body average SAR limit, which is 2 W/kg and 4 W/kg for normal operating mode, first level controlled operating mode, respectively. These limits are cited threshold of temperature rise inside the body. Here, the normal operating mode is an exposure level without any physiological stress to the patient, and is suitable for all patients. In contrast, first level controlled operating mode is exposure level that may cause physiological

stress to the patient, so, medical supervision of the patient is required. Therefore, it is necessary to investigate the SAR with both modes.

As Fig. 7 indicates, at the normal operating mode (in the case of 2 W/kg on whole-body SAR), 10 g average SARs in the uterus and ovary, and in the fetus are below the limit of 10 W/kg. At the first level controlled operating mode (in the case of 4 W/kg on whole-body SAR), 10 g average SARs are also lower than limit of 10 W/kg. Currently, a threshold of adverse effects associated with EM exposure has not been expressly established for fetuses and embryos. Therefore, it

may not be appropriate to estimate as the existing restriction. However from these results, it has confirmed that, the peak 10 g average SARs in the fetus are below the limit in IEC standard under the both operating mode.

4. Conclusions

In this paper, the SAR distributions of two types of woman models (pregnant woman in early period and 26th gestational week woman), which were inserted into two types of birdcage coils, were calculated during MR imaging. The two models of RF coil operate as transmitter and receiver for MR imaging were used; one was a highpass birdcage coil, and the other a lowpass birdcage coil. The summary from the two perspectives are indicated as follows.

1) Local SAR
In order to estimate about the peak SAR of fetal and maternal body, whole-body voxel models were employed. The comparatively high SARs were observed in the muscle and the skin. Especially a high SAR values were observed inside of the armpit and thigh because of existing narrow gap between the tissues. Moreover, the low SAR values were observed around the uterus (for the early period model) and the fetus (for the 26th gestational week model). In addition, it was found from the result that peak SAR values of uterus and fetus are less than 1.0% in comparison with that of maternal body.

2) Average SAR and 10 g average SAR
The average SARs and 10 g average SARs in the pregnant woman models were also investigated. As a consequence, it has been confirmed that fetus and uterus average SARs are less than 30–70% of whole-body average SAR. Subsequently, to compare 10 g average SAR with restriction values in IEC 60601-2-33, the SAR values were normalized to two types of whole-body average SARs; one was 2 W/kg for normal operating mode, and the other was 4 W/kg for first level controlled operating mode. At normal operating mode, 10 g average SARs in the fetus are less than 8–30% of the restriction value which is 10 W/kg for adult threshold. At first level controlled operating mode peak 10 g average SARs in the fetus are less than 17–60% of 10 W/kg.

It is not clear about the affect for fetus exposed to EM waves during MR imaging, because the safety guideline for the fetus has not been established. However, several studies reported the results that thermal effect of the fetus causes growth delay and developmental defect [31], [32]. Therefore, as further study, temperature rise in the fetus due to the RF pulse radiation will be investigated to compare with the threshold dose described in literatures. In addition, the uncertainty assessment on SAR inside fetus will be performed during MR imaging.

References

[1] J. Jin, Electromagnetic analysis and design in magnetic resonance imaging, CRC Press, Boca Raton, 1998.

[2] L.M. Angelone, A. Potthast, F. Segonne, S. Iwaki, J.W. Belliveau, and G. Bonmassar, "Metallic electrodes and leads in simultaneous EEG-MRI: Specific absorption rate (SAR) simulation studies," Bioelectromagnetics, vol.25, pp.285–295, 2004.

[3] J. Chen, Z. Feng, and J. -M. Jin, "Numerical simulation of SAR and B1-field inhomogeneity of shielded RF coils loaded with the human head," IEEE Trans. Biomed. Eng., vol.45, no.5, pp.650–659, 1998.

[4] U.D. Nguyen, J.S. Brown, I.A. Chang, J. Krycia, and M.S. Mirotznik, "Numerical evaluation of heating of the human head due to magnetic resonance imaging," IEEE Trans. Biomed. Eng., vol.51, no.8, pp.1301–1309, Aug. 2004.

[5] D. Simunic, P. Wach, W. Renhart, and R. Stollberger, "Spatial distribution of high-frequency electromagnetic energy in human head during MRI: Numerical results and measurements," IEEE Trans. Biomed. Eng., vol.43, no.1, pp.88–94, Jan. 1996.

[6] C.M. Collins, W. Liu, J. Wang, R. Grütter, J.T. Vaughan, K. Ugurbil, and M.B. Smith, "Temperature and SAR calculations for a human head within volume and surface coils at 64 and 300 MHz," J. Magnetic Resonance Imaging vol.19, pp.650–656, 2004.

[7] International Electromtechnical Commission. International standard, medical equipment-part 2: Particular requirements for the safety of magnetic resonance equipment for medical diagnosis, 2nd revision. Geneva: International Electrotechnical Commission 60601-2-33; pp.29–31, 2002.

[8] A.M. Hubbard, N.S. Adzick, T.M. Crombleholme, B.G. Coleman, L.J. Howel, J.C. Haselgrove, and S. Mahboubi, "Congential chest lesions: Diagnosis and characterization with prenatal MR imaging," Radiology, vol.212, no.1, pp.43–48, July 1999.

[9] R.S. Amin, P. Nickolaidis, A. Kawashima, L.A. Kramer, and R.D. Ernst, "Normal anatomy of the fetus at MR imaging," Radiographics, vol.19, pp.S201–214, Oct. 1999.

[10] D. Levine, "Fetal magnetic resonance imaging," J. Maternal-Fetal and Neonatal Medicine, vol.15, no.2, pp.85–94, Feb. 2004.

[11] J.P. De Wilde, A.W. Rivers, and D.L. Price, "A review of the current use of magnetic resonance imaging in pregnancy and safety implications for the fetus," Progress Biophysics and Molecular Biology, vol.87, pp.335–353, 2005.

[12] M.L. Strydom, K. Caputa, M.A. Stuchly, and P. Gowland, "Numerical modeling interaction of RF field in MRI with a pregnant female," IEEE/ACES Int. Wireless Commun. Appl. Computat. Electromagn. Conf., pp.389–392, April 2005.

[13] J.W. Hand, Y. Li, E.L. Thomas, M.A. Rutherford, and J.V. Hajnal, "Prediction of specific absorption rate calculations in mother and fetus associated with MRI examinations during pregnancy," Magn. Reson. Med., vol.55, pp.883–893, April 2006.

[14] D. Wu, S. Shamsi, J. Chen, and W. Kainz, "Evaluations of specific absorption rate and temperature increase within pregnant female models in magnetic resonance imaging birdcage coils," IEEE Trans. Microw. Theory Tech., vol.54, no.12, pp.4472–4478, Dec.

2006.

[15] T. Nagaoka, T. Togashi, K. Saito, M. Takahashi, K. Ito, and S. Watanabe, "An anatomically realistic whole-body pregnant-woman model and specific absorption rates for pregnant-woman exposure to electromagnetic plane wave from 10 MHz to 2 GHz," Phys. Med. Biol., vol.52, pp.6731–6745, Oct. 2007.

[16] K. Saito, S. Kikuchi, M. Takahashi, K. Ito, and H. Ikehira, "SAR distributions in the abdomen of a pregnant woman generated in a bird cage coil for the MRI system," Proc. Eur. Antennas Propag. Conf., Nov. 2006 [CD-ROM].

[17] T. Togashi, T. Nagaoka, S. Kikuchi, K. Saito, S. Watanabe, M. Takahashi, and K. Ito, "FDTD calculations of specific absorption rate in fetus caused by electromagnetic waves from mobile radio terminal using pregnant woman model," IEEE Trans. Microw. Theory Tech., vol.56, no.2, pp.554–559, Feb. 2008.

[18] K.S. Yee, "Numerical solution of initial boundary values problems involving maxwell's equations in isotropic media," IEEE Trans. Antennas Propag., vol.AP-14, no.3, pp.302–307, May 1966.

[19] Y. Okano, K. Ito, I. Ida, and M. Takahashi, "The SAR evaluation method by a combination of thermographic experiments and biological tissue-equivalent phantoms," IEEE Trans. Microw. Theory Tech., vol.48, no.11, pp.2094–2103, Nov. 2000.

[20] T. Nagaoka, S. Watanabe, K. Sakurai, E. Kunieda, S. Watanabe, M. Taki, and Y. Yamanaka, "Development of realistic high-resolution whole-body voxel models of Japanese adult males and females of average height and weight, and application of models to radio-frequency electromagnetic-field dosimetry," Phys. Med. Biol., vol.49, pp.1–15, 2004.

[21] C. Gabriel, "Compilation of the dielectric properties of body tissues at RF and microwave frequencies," Armstrong Laboratory, Brooks Air Force Technical Report AL/OE-TR-1996-0037, 1996.

[22] F.A. Duck, Physical properties of tissue: A comprehensive reference book, London, Academic Press, 1990.

[23] P.M. Van Den Berg, A.T. De Hoop, A. Segal, and N. Praagmen, "A computational model of the electromagnetic heating of biological tis-sue with application to hyperthermic cancer therapy," IEEE Trans. Biomed. Eng., vol.BME-30, no.12, pp.797–805, Dec. 1983.

[24] J.L. Schepps and K.R. Foster, "The UHF and microwave dielectric properties of normal and tumour tissues: Variation in dielectric properties with tissue water content," Phys. Med. Biol., vol.25, no.6, pp.1149–1159, Nov. 1980.

[25] H. Ochi, E. Yamamoto, K. Sawaya, and S. Adachi, "Analysis of MRI antenna inside an RF shield," IEICE Trans. Commun. (Japanese Edition), vol.J76-B-II, no.2, pp.79–85, Feb. 1993.

[26] C.L. Chin, C.M. Collins, S. Li, B.J. Dardzinski, and M.B. Smith, Bird cage Builder, version 1.0 Copyright Center for NMR Research, Department of Radiology, Penn State University College of Medicine, 1998.

[27] S. Kikuchi, K. Saito, M. Takahashi, K. Ito, and H. Ikehira, "SAR calculations in various parts of pregnant woman during MR imaging," 2007 International Symposium on Antennas and Propagation, pp.434–437, Aug. 2007.

[28] K. Saito, T. Amano, M. Takahashi, K. Ito, and H. Ikehira, "Evaluation of the SAR by two types of RF coils for MRI system," Abstract Book of the Bioelectromagnetics Society 28th Annual Meeting, pp.247–250, June 2006.

[29] P. Dimbylow, "Development of pregnant female, hybrid voxel-mathmatical models and their application to the dosimetry of applied magnetic and electric fields at 50 Hz," Phys. Med. Biol., vol.51, pp.2383–2394, Nov. 2006.

[30] IEEE Recommended Practice for Measurements and Computations of Radio Frequency Electromagnetic Fields with Respect to Human Exposure to Such Fields, 100 kHz–300 GHz, IEEE Standard C95.3-2002, 2002.

[31] J.M. Graham, M.J. Edwards, and M.J. Edwards, "Teratogen update: Gestational effects of maternal hyperthermia due to febrile illnesses and resultant patterns of defects in humans," Teratology, vol.58, pp.209–221, 1998.

[32] M.J. Edwards, R.D. Saunders, and K. Shiota, "Effects of heat on embryos and foetuses," Int. J. Hyperthermia, vol.19, no.3, pp.295–324, 2003.

Satoru Kikuchi was born in Aomori, Japan, in March 1983. He received the B.E. and M.E. degrees both in electrical engineering from Chiba University, Chiba, Japan, in 2005 and 2007, respectively. He and is currently working toward the Ph.D. degree at Chiba University. His main interests include research on evaluation of the interaction between electromagnetic (EM) field and the human body by use of numerical human model and experimental phantoms, and analysis and design of antennas for microwave hyperthermia. Mr. Kikuchi is a member of the IEEE, the Japanese Society for Thermal Medicine, and the Bioelectromagnetics Society.

Kazuyuki Saito was born in Nagano, Japan, in May 1973. He received the B.E., M.E. and D.E. degrees all in electronic engineering from Chiba University, Chiba, Japan, in 1996, 1998 and 2001, respectively. He is currently an Assistant Professor with the Research Center for Frontier Medical Engineering, Chiba University. His main interest is in the area of medical applications of the microwaves including the microwave hyperthermia. He received the IEICE AP-S Freshman Award, the Award for Young Scientist of URSI General Assembly, the IEEE AP-S Japan Chapter Young Engineer Award, the Young Researchers' Award of IEICE, and the International Symposium on Antennas and Propagation (ISAP) Paper Award in 1997, 1999, 2000, 2004, and 2005 respectively. Dr. Saito is a member of the IEEE, the Institute of Image Information and Television Engineers of Japan (ITE), and the Japanese Society for Thermal Medicine.

Masaharu Takahashi was born in Chiba, Japan, on December, 1965. He received the B.E. degree in electrical engineering in 1989 from Tohoku University, Miyagi, Japan, and the M.E. and D.E. degrees both in electrical engineering from Tokyo Institute of Technology, Tokyo, Japan, in 1991 and 1994 respectively. He was a Research Associate from 1994 to 1996, an Assistant Professor from 1996 to 2000 at Musashi Institute of Technology, Tokyo, Japan, and an Associate Professor from 2000 to 2004 at Tokyo University of Agriculture and Technology, Tokyo, Japan. He is currently an Associate Professor at the Research Center for Frontier Medical Engineering, Chiba University, Chiba, Japan. His main interests are electrically small antennas, planar array antennas, and electromagnetic compatibility. He received the IEEE Antennas and Propagation Society (IEEE AP-S) Tokyo chapter young engineer award in 1994. Dr. Takahashi is a senior member of the IEEE.

Koichi Ito received the B.S. and M.S. degrees from Chiba University, Chiba, Japan, in 1974 and 1976, respectively, and the D.E. degree from the Tokyo Institute of Technology, Tokyo, Japan, in 1985, all in electrical engineering. From 1976 to 1979, he was a Research Associate at the Tokyo Institute of Technology. From 1979 to 1989, he was a Research Associate at Chiba University. From 1989 to 1997, he was an Associate Professor at the Department of Electrical and Electronics Engineering, Chiba University, and is currently a Professor at the Graduate School of Engineering, Chiba University. He has been appointed as one of the Deputy Vice-Presidents for Research, Chiba University, since April 2005. In 1989, 1994, and 1998, he visited the University of Rennes I, France, as an Invited Professor. Since 2004 he has been appointed as an Adjunct Professor to Institute of Technology Bandung (ITB), Indonesia. His main research interests include analysis and design of printed antennas and small antennas for mobile communications, research on evaluation of the interaction between electromagnetic fields and the human body by use of numerical and experimental phantoms, microwave antennas for medical applications such as cancer treatment, and antennas for body-centric wireless communications. Dr. Ito is a Fellow of the IEEE, a member of the American Association for the Advancement of Science, the Institute of Image Information and Television Engineers of Japan (ITE) and the Japanese Society for Thermal Medicine (formerly, Japanese Society of Hyperthermic Oncology). He served as Chair of the Technical Group on Radio and Optical Transmissions, ITE from 1997 to 2001 and Chair of the Technical Group on Human Phantoms for Electromagnetics, IEICE from 1998 to 2006. He also served as Chair of the IEEE AP-S Japan Chapter from 2001 to 2002 and TPC Co-Chair of the 2006 IEEE International Workshop on Antenna Technology (iWAT2006). He currently serves as General Chair of the iWAT2008 to be held in Chiba, Japan in 2008, Vice-Chair of the 2008 International Symposium on Antennas and Propagation (ISAP2008) to be held in Taiwan in 2008 and as an Associate Editor for the IEEE Transactions on Antennas and Propagation. He also serves as a Distinguished Lecturer and an AdCom member for the IEEE Antennas and Propagation Society since January 2007.

Hiroo Ikehira was born in Kyoto, Japan, in February 1955. He received the Medical License degree from Kobe University in 1980, the M.D. and Ph.D. degree in medicine from Chiba University in 1987. He was a Researcher from 1980 to 1988, a Senior Researcher from 1989 to 1998, a General Manager at the Laboratory of Molecule Information, the National Institute of Radiological Sciences (NIRS). From 1990 to 1997, he became an assistant professor with the Department of Radiology, Chiba University Hospital. From 1998–2000, he was an associate professor with the Faculty of Medicine, Chiba University. In 1982, he visited Faculty of Medicine at the University of Aberdeen, UK, as Resident. In 1987, he was a Visiting Scientist with the Lawrence Berkeley National Laboratory, California, USA. He is currently a Deputy Director at the Biophysics Group of Molecular Imaging Center, NIRS, an affiliate professor with the Graduate School of Medicine, Chiba University, and a lecturer with Graduate School of Frontier Sciences, University of Tokyo. His main research interest is the bioimaging with magnetic resonance imaging (MRI) system. Dr. Ikehira is member of the International Society for Magnetic Resonance in Medicine (ISMRM).